nature geoscience

Article

https://doi.org/10.1038/s41561-026-01965-8

Stratospheric cooling and amplification of radiative forcing with rising carbon dioxide

Received: 13 September 2025

Accepted: 27 February 2026

Published online: 11 May 2026

Check for updates

Sean Cohen ✉, Robert Pincus & Lorenzo M. Polvani

The cooling of the stratosphere in response to increasing carbon dioxide concentration is a fingerprint of human effects on climate. However, the mechanisms that control the magnitude and vertical structure of this cooling have not been clear. Here we use idealized models of spectroscopy and radiative transfer to explain the sensitivity of stratospheric temperature to carbon dioxide concentration. We find that stratospheric cooling is mainly driven by the distribution of mass absorption coefficients in the primary carbon dioxide band and modulated by the longwave cooling of water vapour and ozone in other parts of the spectrum. These spectral mechanisms explain why the stratosphere cools more aloft than it does below, why each doubling of carbon dioxide yields roughly 0 to 8 degrees Kelvin of cooling across the depth of the stratosphere and why stratospheric cooling increases the top of atmosphere radiative forcing of carbon dioxide by about 50%. This theory implies that stratospheric cooling is not a fundamental consequence of increasing the optical thickness of a greenhouse gas but rather the unique result of the spectroscopy of that gas.

Stratospheric cooling is one of the most robust signals of carbon dioxide (CO_2)-induced climate change. Since some of the earliest attempts to simulate the effects of increased CO_2 concentrations on Earth's atmosphere[1,2], it has been clear across both observations and models[3–11] that increases in atmospheric carbon dioxide cause globally averaged stratospheric temperatures to decrease. This cooling, which occurs on much shorter timescales than the warming of the surface and troposphere[4], is one of the most directly observable effects of increased CO_2 concentrations and thus a harbinger of global climate change[9,10].

Because heating by circulation integrates to zero in the global mean, Earth's global-averaged temperature is well approximated by radiative convective equilibrium (RCE)[1,2] in the troposphere and by radiative equilibrium in the stratosphere: CO_2 and water vapour cool the stratosphere by emitting infrared (that is, longwave) radiation, and ozone primarily heats the stratosphere by absorbing sunlight (that is, shortwave radiation) but also cools via the infrared[12,13]. Single-column RCE simulations offer a useful context in which to study stratospheric cooling because their reduced dimensionality allows the dominant physics in this process, radiation, to be explicitly computed. Figure 1a shows the steady-state temperature profiles simulated by one such RCE model, Konrad[14], across a range of CO_2 concentrations. Surface temperature and ozone concentration are fixed at their global-mean values, and radiative transfer is computed using the atmospheric radiative transfer simulator (ARTS), a line-by-line radiative transfer model[15]. By construction, tropospheric temperatures, which are set by the moist adiabat originating at the (fixed) surface temperature, also remain fixed to their pre-industrial values. Despite these idealizations, single-column RCE broadly reproduces observed and simulated trends in global-mean annual stratospheric temperature from 1980 to 2014 (Fig. 1c).

Several well-known features of CO_2-induced stratospheric cooling are evident. First, stratospheric temperature changes are largest near the stratopause (≈1 hPa)[9], where each doubling of CO_2 yields roughly 8K of cooling (Fig. 1b)[1,16–18]; near the tropopause, the steady-state temperature is hardly affected by changes in CO_2[9] (this is the case even well above the pressure level where convective adjustment stops occurring; Extended Data Fig. 1). Second, stratospheric temperature changes roughly logarithmically with CO_2 concentration, with each doubling of CO_2 yielding roughly the same change in temperature at a given pressure level in the stratosphere (Fig. 1b)[1,18]. These changes in stratospheric temperature have important implications for Earth's energy budget: increases in CO_2 concentration induce an energy imbalance at the top of the atmosphere, or radiative forcing, which stratospheric cooling amplifies by ≈40%–60% (relative to its instantaneous value)[3,19–21].

Lamont-Doherty Earth Observatory, Columbia University, Palisades, NY, USA. ✉e-mail: sean.cohen@columbia.edu

https://doi.org/10.1038/s41561-026-01965-8

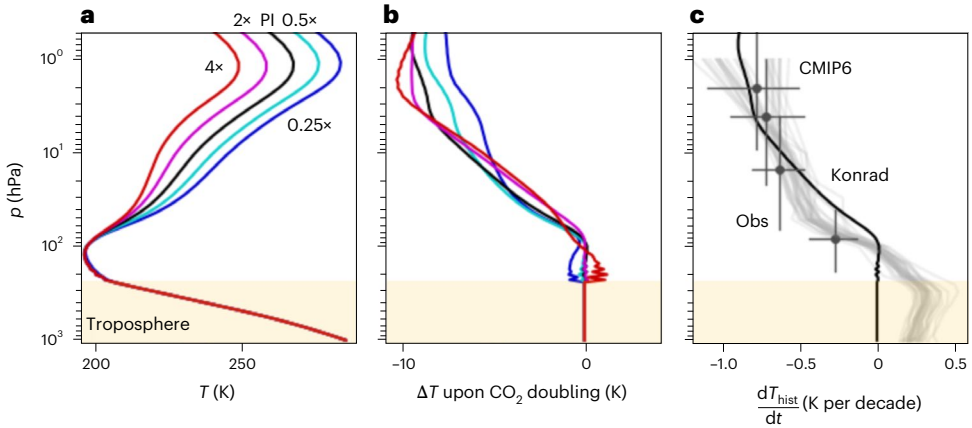

Fig. 1 | Increases in CO_2 cool the global-mean stratosphere. a, RCE simulations in Konrad (using ARTS) under pre-industrial CO_2 concentration (black) and under subsequent doublings (warmer colours) and halvings (cooler colours) of CO_2 concentration from pre-industrial (PI) levels. Convective adjustment stops occurring at ≈200 hPa (yellow). **b**, The stratospheric temperature response upon doubling CO_2 from various initial CO_2 concentrations (same line colours). **c**, Global-mean annual temperature trend from 1980 to 2014 in 36 CMIP6 models (light grey lines) and in the SSU-AMSU (Stratospheric Sounding Unit) and MSU4-AMSU (Microwave Sounding Unit) NOAA/STAR (Center for Satellite Applications and Research) dataset (dark grey dots denote mean value, vertical bars denote the vertical weighting of the satellite measurements and horizontal bars show 2-sigma statistical uncertainties[44,45]). Differencing across RCE simulations in Konrad that use CO_2 concentrations of 339 ppm (1980) and 399 ppm (2014) broadly reproduces these trends (black line).

Existing arguments qualitatively explain why increases in CO_2 cause the stratosphere to cool. When CO_2 concentration rises, atmospheric emissivity increases such that a lower temperature is needed to achieve the same longwave emission by CO_2 (ref. 5). Because shortwave heating by ozone stays roughly fixed, the stratosphere cools to remain in radiative equilibrium[4,22]. This reasoning, however, offers little insight into the magnitude and vertical distribution of cooling within the stratosphere and how this cooling might depend on other atmospheric state variables such as temperature or the concentration of CO_2 and other greenhouse gases. This limited understanding largely stems from a reliance on grey or quasi-grey radiation approaches, which simulate unrealistic stratospheric temperature profiles and thus offer limited insight into the drivers of stratospheric cooling[23].

Here we show that the spectroscopy of carbon dioxide is key to understanding the physical mechanisms which drive stratospheric cooling. We address three key questions: (1) why does the stratosphere cool more aloft than it does below? (2) Why does a doubling of CO_2 yield roughly 8K of cooling at the stratopause? (3) Why does stratospheric cooling increase the top of atmosphere (TOA) radiative forcing of CO_2 by about 50%? These facts have been known for decades, yet no theoretical understanding is available to explain them. Using idealized models of spectroscopy and radiative transfer, we demonstrate that stratospheric cooling emerges because rising CO_2 levels increase the fraction of the CO_2 band that can effectively emit longwave radiation to space. The magnitude and vertical structure of these changes provide quantitative answers to Questions (1)–(3), offering a more robust explanation for how and why the stratosphere cools when atmospheric carbon dioxide increases.

Connection to the spectroscopy of CO_2

Throughout most of the stratosphere, radiative exchange with the surface and the surrounding atmosphere largely cancel such that heating by CO_2 (H_{CO_2}) is well approximated by considering only longwave emission to space (Extended Data Fig. 2). The cooling-to-space (CTS) approximation[24,25] implies that CO_2's longwave heating rate H_{CO_2} at a given pressure level p is controlled by both the emissivity of the CO_2 band and the local temperature T (ref. 26):

$$H_{CO_2} = -\frac{2g}{pc_p}\pi B(T,\nu_0)l(p,q) \quad (1)$$

Here g is the acceleration due to gravity, c_p is the specific heat of air and $B(T,\nu_0)$ is the Planck function evaluated at the wavenumber at the centre of the CO_2 band (ν_0, 667.5 cm^{-1}). For a given CO_2 concentration q, the spectrally integrated weighting function

$$l(p,q) = \int_{CO_2} \tau_\nu e^{-\tau_\nu} d\nu \quad (2)$$

quantifies the emissivity of the CO_2 band, measuring how many wavenumbers ν have an optical depth $\tau_\nu(p,q)$ near unity ($\tau_\nu e^{-\tau_\nu}$ peaks at $\tau_\nu = 1$) and thus substantially contribute to H_{CO_2} (Methods). Sometimes called the effective emitting width[26,27], $l(p,q)$ might also be referred to as the Goldilocks width because it quantifies the portion of the spectrum (in cm^{-1}) that is neither too optically thick nor too optically thin to effectively cool to space from pressure level p.

When CO_2 concentration rises, τ_ν (which is $\propto qp^2$) increases, causing CO_2's Goldilocks width to change in a height-dependent manner; these changes are controlled by CO_2's spectroscopy[26]. Consider the mass absorption coefficient of CO_2 $k_{ref}(\nu)$ at 100 hPa (Fig. 2a, grey), which has complicated but well-understood spectral behaviour[28]. This distribution is qualitatively similar at other pressures but shifted to larger or smaller values by pressure broadening[29]. Sorting the absorption coefficients on each side of the band (Fig. 2b) reveals that the distribution becomes more peaked near the band centre, and binning the logarithm of $k_{ref}(\nu)$ (Fig. 2c, grey) quantifies how many wavenumbers in the CO_2 band have a given mass absorption coefficient (or one quite close to it) at the reference pressure of 100 hPa. Because emission at p is dominated by the absorption coefficients near unity optical depth, Goldilocks width $l(p,q)$ can be approximated by evaluating $l(k_{ref})$ at the value yielding $\tau_\nu = 1$ at pressure p and CO_2 concentration q (Methods).

Simple parameterizations of the spectroscopy of CO_2 (in which $\ln(k_{ref})$ decays linearly in ν away from the centre of the CO_2 band; Fig. 2a, orange) have been useful in understanding how CO_2 affects tropospheric longwave emission and the top of atmosphere radiation budget[26,27,29–31]. However, this distribution of absorption coefficients causes l to transition abruptly from a finite value to zero at the maximum value of k_{ref} (Fig. 2c, orange), producing stratospheric cooling that is amplified near this transition and near zero elsewhere (much like transitions in tropospheric relative humidity produce local maxima in longwave emission by water vapour[32]; Extended Data Fig. 3). The distribution of absorption coefficients is better represented via a

https://doi.org/10.1038/s41561-026-01965-8

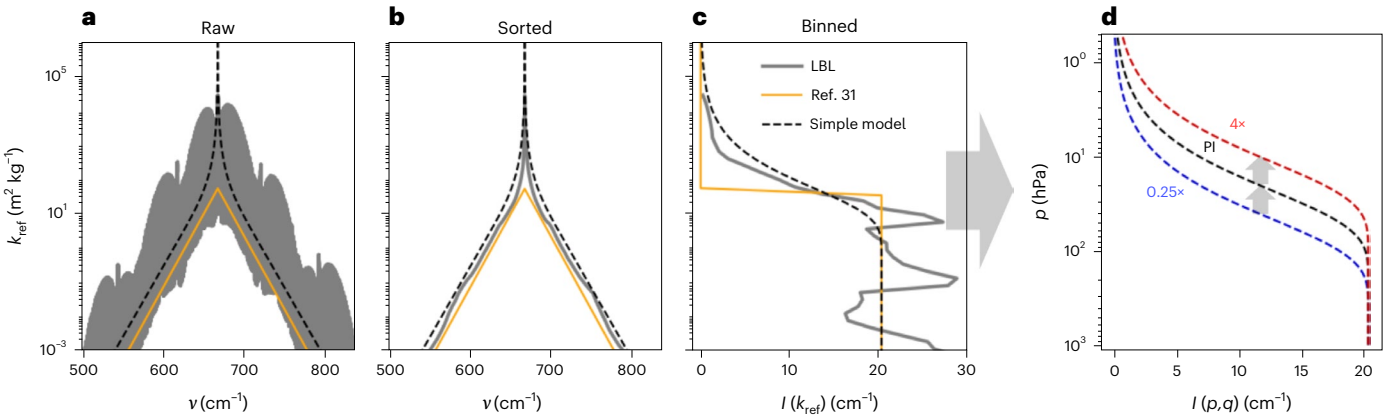

Fig. 2 | CO_2's spectroscopy drives stratospheric cooling. a,**b**, CO_2's mass absorption coefficient $k_{ref}(\nu)$ at 100 hPa (grey, derived from ARTS) (**a**) and sorted from largest to smallest on each side of the CO_2 band (**b**). **c**, Binning $k_{ref}(\nu)$ in log space approximates CO_2's Goldilocks width l. **a**–**c**, Simple parameterizations of $k_{ref}(\nu)$ (for example, from ref. 31, orange) capture the behaviour $k_{ref}(\nu)$ at the edges of the CO_2 band but miss the rapid increase of absorption at the centre of the CO_2 band. We refine these idealizations by parameterizing l as a function of $k_{ref}(\nu)$ (dashed black) and **d** as a function of pressure. **d**, When CO_2 concentration rises (dashed blue → dashed black → dashed red), CO_2's Goldilocks width increases at most pressure levels in the stratosphere.

parameterization, which reproduces $l(k_{ref})$ near the band's peak (Fig. 2a–c, dashed black), the details of which are outlined in Methods and Extended Data Table 1.

Changes in Goldilocks width with CO_2 concentration are controlled by the distribution of mass absorption coefficients in the CO_2 band—in particular how this distribution changes from peak to edge (Fig. 2c). At pressures greater than about 50 hPa, CO_2 emits to space primarily from the edges of the CO_2 band because this is where CO_2's less absorbent wavenumbers are near unity optical depth. Here CO_2's Goldilocks width is large (Fig. 2c) but essentially invariant to changes in CO_2 concentration (Fig. 2d). At pressures less than 50 hPa, in contrast, emission to space is dominated by the more absorbent wavenumbers near the peak of the CO_2 band. Here $l(p, q)$ is relatively small but increases sharply with CO_2 concentration. It is this increase in l that ultimately drives stratospheric cooling.

Quantifying stratospheric cooling

Changes in Goldilocks width drive stratospheric temperature change by altering emissions across the longwave spectrum. As CO_2 concentration changes, CO_2's longwave heating rate H_{CO_2} adjusts according to the corresponding changes in Goldilocks width and temperature that these changes in concentration induce:

$$\frac{\mathrm{d}\ln H_{CO_2}}{\mathrm{d}\ln q} = \underbrace{\frac{\mathrm{d}\ln l(p,q)}{\mathrm{d}\ln q}}_{l\text{–driven}} + \underbrace{\frac{\mathrm{d}\ln B(T,\nu_0)}{\mathrm{d}\ln T}\frac{\mathrm{d}\ln T}{\mathrm{d}\ln q}}_{T\text{–driven}} \quad (3)$$

Because global-mean annual stratospheric temperature is primarily controlled by radiative equilibrium, any transient change in longwave heating by CO_2 must eventually be balanced by an equal and opposite change in longwave and shortwave heating by other radiatively active gases H_o, namely ozone and water vapour (an assumption which also holds locally under fixed dynamical heating[16,33]):

$$\frac{\mathrm{d}H_{CO_2}}{\mathrm{d}\ln q} = -\frac{\mathrm{d}H_o}{\mathrm{d}\ln q} \quad (4)$$

Whereas shortwave heating is largely invariant to changes in CO_2 concentration[34] (Extended Data Fig. 4), longwave cooling, which is strongly influenced by changes in stratospheric temperature, is not. As CO_2 concentration rises, longwave cooling by CO_2 increases (Fig. 3a); the resulting drop in stratospheric temperature decreases the longwave cooling of all radiatively active gases (that is, CO_2, H_2O and O_3; Fig. 3b) such that the stratosphere remains in radiative equilibrium (Fig. 3c,d). Consequently, longwave cooling by other gases reduces stratospheric cooling[35].

Together, equations (3) and (4) imply that stratospheric cooling is driven by changes in CO_2's Goldilocks width and damped by the compensating reduction in the longwave cooling of water vapour and ozone:

$$\Delta\ln T \approx -\left(\frac{\eta}{\alpha}\right)\Delta\ln l \quad (5)$$

Here $\alpha = \frac{\mathrm{d}\ln B(T,\nu_0)}{\mathrm{d}\ln T} \approx 4$ is a source scaling that indicates the rate at which emission by CO_2 increases with temperature[25] (Methods). The non-dimensional quantity $\eta = \frac{\mathrm{d}H_{CO_2}}{\mathrm{d}T} / \frac{\mathrm{d}(H_{CO_2}+H_o)}{\mathrm{d}T} \approx 0.4$ is a 'spectral efficiency' whose value is determined empirically from radiative transfer calculations (Methods); for a given change in stratospheric temperature, η measures what fraction of the total change in longwave cooling comes from CO_2 rather than from ozone and water vapour. When the concentration of ozone and water vapour is constant, H_o scales roughly linearly with local temperature (Extended Data Fig. 5). In reality, the chemical reactions that produce and destroy ozone, the primarily shortwave absorber in the stratosphere, are themselves a function of temperature[36], meaning stratospheric cooling can alter the concentration of ozone and, by extension, the shortwave heating it produces. Because changes in global-mean stratospheric ozone due to a quadrupling of CO_2 are quite small[37], we neglect this feedback in the present study (along with other feedbacks that might change the concentration of ozone and water vapour, such as the acceleration of the Brewer–Dobson circulation[38]), though these influences could be incorporated as an additional input to $\frac{\mathrm{d}H_o}{\mathrm{d}T}$.

Equation (5) captures the magnitude and vertical structure of CO_2-induced stratospheric cooling as computed by RCE simulations using line-by-line radiative transfer (Fig. 4b). The change in CO_2's Goldilocks width (Fig. 4a) in particular offers quantitative insight into how and why the stratosphere cools.

Because α and η vary little across the depth of the stratosphere (about 15% and 30%, respectively; Extended Data Fig. 6), the vertical structure of stratospheric cooling is primarily controlled by how CO_2's Goldilocks width changes with CO_2 concentration. Evident in the similarity between panels (a) and (b) of Fig. 4, this explains both why the stratosphere cools more aloft than it does below and why this cooling depends roughly logarithmically on CO_2 concentration: $\frac{\mathrm{d}\ln l}{\mathrm{d}\ln q}$ grows

https://doi.org/10.1038/s41561-026-01965-8

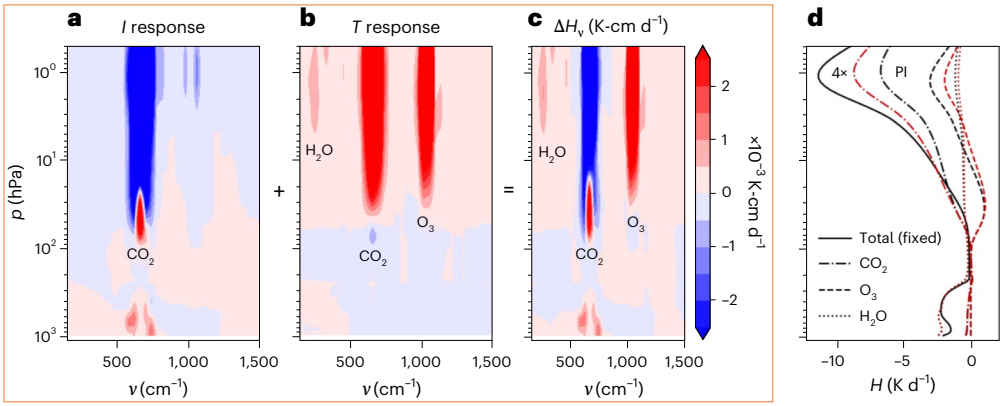

Fig. 3 | Emission by O_3 and H_2O dampens stratospheric cooling. a, When CO_2 concentration rises from PI to 4 × PI, the spectrally resolved longwave heating rate H_ν decreases in the CO_2 absorption band, causing the stratosphere to cool. **b**, This cooling increases H_ν in the absorption bands of all radiatively active gases. **c**, Cooling continues until the stratosphere regains radiative equilibrium. **d**, Because shortwave heating is largely invariant to changes in q, the total spectrally integrated longwave heating at each pressure level (solid black) is the same as it was before the increase in q.

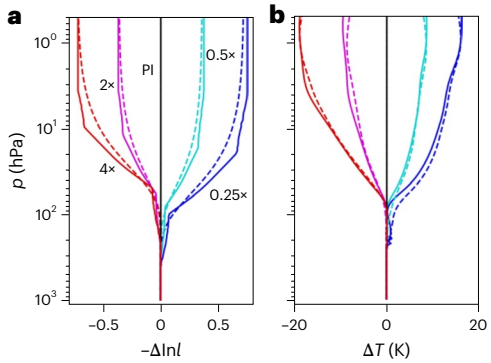

Fig. 4 | Changes in Goldilocks width control the vertical structure of stratospheric cooling. a,**b**, Fractional change in CO_2's Goldilocks width (**a**) and associated stratospheric temperature change (**b**) from pre-industrial conditions (black) under subsequent doublings (warmer colours) and halvings (cooler colours) of CO_2 concentration. We compare our idealized model (dashed) to RCE simulations in Konrad (solid), which are smoothed in **a**.

as pressure falls and is roughly constant at pressures lower than 10 hPa (Fig. 4a), so $\frac{\mathrm{d}\ln T}{\mathrm{d}\ln q}$ shares the same properties (Fig. 4b). Furthermore, this proportionality suggests that changes in CO_2 concentration do not affect stratospheric temperature in ultra-high CO_2 atmospheres. Whereas CO_2's Goldilocks width is roughly logarithmically dependent on q, as q increases the pressure level p^* at which $\Delta\ln l \approx 0$ (and thus $\Delta\ln T \approx 0$) falls according to $p^* \propto q^{-1/2}$ (this is one reason why stratospheric temperature is not precisely logarithmically dependent on CO_2 concentration; Fig. 6 of ref. 18). More generally, equation (5) suggests that increases in CO_2 concentration would warm the stratosphere rather than cool it if CO_2's spectroscopy were different: if l were to change with k_{ref} such that $\Delta\ln l$ was no longer strictly greater than zero, increases in CO_2 concentration would warm at least some parts of stratosphere.

The magnitude of maximum cooling from a doubling of CO_2 (which occurs near the stratopause) is determined by the magnitudes of α, η and $\Delta\ln l$:

$$\Delta T = -\frac{\eta}{\alpha}(\Delta\ln l)\,T \approx -\frac{0.4}{4}(0.3)(260\,\mathrm{K}) \approx -8\,\mathrm{K} \qquad (6)$$

implying that, in the absence of any change in longwave heating by other gases ($\eta = 1$), stratospheric cooling would be more than twice as large (Extended Data Fig. 7).

How stratospheric cooling amplifies radiative forcing

One key consequence of CO_2-induced stratospheric cooling is its impact on CO_2's radiative forcing[3,39–41]. When CO_2 concentration increases, surface emission (and tropospheric emission by water vapour) at the edges of the CO_2 band is masked and replaced by stratospheric emission from the centre of the CO_2 band[30,31]. The TOA instantaneous radiative forcing (IRF) is thus controlled by the temperature contrast between the surface (or lower troposphere) and the stratosphere[42]. Stratospheric cooling amplifies this temperature contrast, causing the TOA stratosphere-adjusted radiative forcing (SARF) to be greater than the IRF[18]. The TOA effective radiative forcing (ERF) of CO_2—which accounts for all adjustments (for example, changes in clouds and circulation), not only stratospheric cooling—is nearly equal to SARF in comprehensive GCMs[43] and precisely equal to SARF in single-column RCE frameworks where stratospheric cooling is the only adjustment.

Effective radiative forcing can be computed from equation (5) by considering how emission from the CO_2 band changes when CO_2 concentration increases:

$$\mathrm{ERF} = 2\pi\left(l_0 B(\bar{T}, \nu_0)\Delta\ln q - \int_0^{\bar{p}} \Delta l\,(1-\eta)\,B(T,\nu_0)\mathrm{d}\ln p\right) \qquad (7)$$

Here $\bar{p}$ is the average emission pressure at the edges of the CO_2 band[31] and $\bar{T}$ is the temperature at $\bar{p}$ (Methods).

The first term in equation (7) represents the masked surface and tropospheric emission by water vapour while the second represents the change in stratospheric emission by CO_2 ($\Delta l = 0$ in the troposphere) due to changes in CO_2's Goldilocks width and the resulting stratospheric adjustment. Using equation (7), we numerically estimate IRF, ERF and the magnitude of the stratospheric adjustment (ERF − IRF) at various surface temperatures for a doubling of CO_2 from pre-industrial, finding good agreement with line-by-line radiative transfer calculations in ARTS (Fig. 5). These estimates only capture the portion of the radiative forcing originating from the wavenumbers in the CO_2 band, although this accounts for at least 85% of the total radiative forcing in all cases we considered.

Curiously, emission from the CO_2 band alone is a useful proxy for ERF (equation (7)) even though stratospheric cooling reduces emission to space by water vapour and ozone as well. This apparent contradiction can be resolved by noting that while longwave cooling by CO_2 is well approximated by cooling-to-space (Extended Data Fig. 2), longwave cooling by ozone, particularly in the lower stratosphere, is not (Extended Data Fig. 5a). This difference emerges primarily from

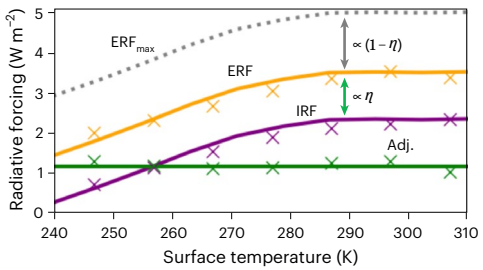

Fig. 5 | Spectral efficiency controls the magnitude of the stratospheric adjustment. Radiative forcing across the CO_2 band due to doubling of CO_2 from pre-industrial CO_2 concentration at various surface temperatures. Line-by-line computations in Konrad (crosses) are compared to equation (7) (lines). Because $\eta \approx 0.4$, the effective radiative forcing (orange) falls about halfway between the instantaneous radiative forcing (purple, $\eta = 0$) and a theoretical maximum radiative forcing (grey, equation (8), $\eta = 1$) where ozone and water vapour do not mute stratospheric cooling. The magnitude of the stratospheric adjustment (green) is largely invariant to changes surface temperature.

ozone's unique concentration profile. Unlike CO_2, which is well mixed, ozone's concentration profile peaks near 10 hPa, meaning ozone's optically thick wavenumbers in the lower stratosphere are more heavily impacted by emission from the surface and troposphere than they are by emission to space (Methods); this is why longwave cooling by ozone is actually negative (that is, net heating) in the lower stratosphere (Fig. 3d). As a result, H_o, which is almost entirely controlled by ozone, is largely untethered from cooling to space in the lower stratosphere (Extended Data Fig. 5b). This means stratospheric emission to space, which comes primarily from the lower stratosphere, is dominated by CO_2, making changes in emission from the CO_2 band a suitable first-order proxy for ERF as a whole (Extended Data Fig. 8; Methods provide a more complete analysis).

Near present-day conditions, IRF is ≈2.2 W m^{-2}, ERF is ≈3.4 W m^{-2} and the adjustment is ≈1.2 W m^{-2}. As the surface cools, less surface/tropospheric emission is masked by CO_2, so IRF and ERF decrease[31,42]; however, because the radiative physics governing the stratosphere are largely independent of the surface, the adjustment remains ≈1.2 W m^{-2}.

Because IRF is set by the temperature contrast between the surface/troposphere and the stratosphere[31,42], it depends on latitude, stratospheric temperature and CO_2 concentration. The adjustment, in contrast, depends only on the amount of stratospheric cooling, perhaps partially explaining why the stratospheric adjustment is nearly invariant zonally and meridionally in the CMIP6 (Coupled Model Intercomparison Project) multi-model mean (Fig. 6d of ref. 19). However, dynamical heating does not remain fixed under changes in CO_2 (ref. 38), so local changes in stratospheric temperature are not entirely radiatively constrained. Because stratospheric temperature changes roughly logarithmically with q, the adjustment also changes relatively little with CO_2 concentration (≈10% per CO_2 doubling; Extended Data Fig. 9). This implies that clouds (which this study neglects) affect ERF and IRF by lowering the tropospheric emission temperature that CO_2 masks but are unlikely to affect the stratospheric adjustment.

Two limiting cases of η, the stratosphere's spectral efficiency, illustrate why near present-day conditions, stratospheric adjustment increases the TOA radiative forcing by about 50% compared to its instantaneous value. If longwave emission across the spectrum were very sensitive to stratospheric temperature ($\eta \approx 0$), relatively little cooling would be needed to achieve radiative equilibrium after a change in CO_2 concentration. In this limit, the stratospheric adjustment goes to zero, and ERF and IRF are equivalent to the value from ref. 31, ≈2.1 W m^{-2}.

In contrast, if stratospheric emission were dominated by the CO_2 band ($\eta \approx 1$), any fractional increase in CO_2's Goldilocks width (that is, $l(p, q)$) would be met by an equal and opposite fractional decrease in emission from those same wavenumbers. In this limit (Fig. 5, dotted grey), the adjustment would entirely cancel any additional stratospheric emission from the CO_2 band and ERF would be given by the masked surface term alone:

$$\mathrm{ERF}_{\max} = 2\pi l_0 B(\bar{T}, \nu_0)\Delta \ln q \approx 5.0\ \mathrm{W\,m^{-2}} \quad (8)$$

Earth's present-day atmosphere, which has $\eta \approx 0.4$, operates roughly halfway between these extremes. Because changes in temperature induce a similar change in the heating rate of CO_2 as they do the combined heating rate of ozone and water vapour, the stratospheric adjustment roughly halves the additional stratospheric emission from the centre of the CO_2 band. This implies:

$$\mathrm{ERF} \approx \eta \mathrm{ERF}_{\max} + (1-\eta)\mathrm{IRF} \approx 3.3\ \mathrm{W\,m^{-2}} \quad (9)$$

suggesting that the roughly 50% increase in TOA radiative forcing from the stratospheric adjustment emerges from the fact that $\eta \approx 0.4$ in most of the stratosphere.

Online content

Any methods, additional references, Nature Portfolio reporting summaries, source data, extended data, supplementary information, acknowledgements, peer review information; details of author contributions and competing interests; and statements of data and code availability are available at https://doi.org/10.1038/s41561-026-01965-8.

References

1. Manabe, S. & Wetherald, R. T. Thermal equilibrium of the atmosphere with a given distribution of relative humidity. *J. Atmos. Sci.* **24**, 241–259 (1967).
2. Manabe, S. & Wetherald, R. T. The effects of doubling the CO_2 concentration on the climate of a general circulation model. *J. Atmos. Sci.* **32**, 3–15 (1975).
3. Hansen, J., Sato, M. & Ruedy, R. Radiative forcing and climate response. *J. Geophys. Res.: Atmos.* **102**, 6831–6864 (1997).
4. Ramaswamy, V. et al. Stratospheric temperature trends: Observations and model simulations. *Rev. Geophys.* **39**, 71–122 (2001).
5. Ramaswamy, V. & Schwarzkopf, M. D. Effects of ozone and well-mixed gases on annual-mean stratospheric temperature trends. *Geophys. Res. Lett.* **29**, 21–1–21–4 (2002).
6. Shine, K. P. et al. A comparison of model-simulated trends in stratospheric temperatures. *Q. J. R. Meteorolog. Soc.* **129**, 1565–1588 (2003).
7. Thompson, D. W. J. et al. The mystery of recent stratospheric temperature trends. *Nature* **491**, 692–697 (2012).
8. Fujiwara, M., Manney, G., Gray, L. & Wright, J. *The Sparc S-RIP Activity: Sparc Reanalysis Intercomparison Project (S-RIP) Final Report* (2022).
9. Santer, B. D. et al. Exceptional stratospheric contribution to human fingerprints on atmospheric temperature. *Proc. Natl Acad. Sci. USA* **120**, e2300758120 (2023).
10. Santer, B. D. et al. A search for human influences on the thermal structure of the atmosphere. *Nature* **382**, 39–46 (1996).
11. Mitchell, D., Lo, E., Seviour, W., Haimberger, L. & Polvani, L. The vertical profile of recent tropical temperature trends: persistent model biases in the context of internal variability. *Environ. Res. Lett.* **15** (2020).
12. Pierrehumbert, R. T. *Principles of Planetary Climate* (2010).
13. Neelin, J. D. *Climate Change and Climate Modeling* (2011).
14. Kluft, L., Dacie, S., Buehler, S. A., Schmidt, H. & Stevens, B. Re-examining the first climate models: climate sensitivity of a modern radiative–convective equilibrium model. *J. Climate* **32**, 8111–8125 (2019).

15. Buehler, S. A. et al. *The Atmospheric Radiative Transfer Simulator Arts, Version 2.6—Deep Python Integration* (2024).
16. Fels, S. B., Mahlman, J. D., Schwarzkopf, M. D. & Sinclair, R. W. Stratospheric sensitivity to perturbations in ozone and carbon dioxide: radiative and dynamical response. *J. Atmos. Sci.* **37**, 2265–2297 (1980).
17. Rind, D., Suozzo, R., Balachandran, N. K. & Prather, M. J. Climate change and the middle atmosphere. Part I: the doubled CO_2 climate. *J. Atmos. Sci.* **47**, 475–494 (1990).
18. Mitevski, I. et al. State dependence of CO_2 effective radiative forcing from 1/16 × to 16 × co2. *J. Clim.* https://journals.ametsoc.org/view/journals/clim/aop/JCLI-D-24-0387.1/JCLI-D-24-0387.1.xml (2025).
19. Smith, C. J. et al. Effective radiative forcing and adjustments in cmip6 models. *Atmos. Chem. Phys.* **20**, 9591–9618 (2020).
20. Pincus, R. et al. Benchmark calculations of radiative forcing by greenhouse gases. *J. Geophys. Res.: Atmos.* **125**, e2020JD033483 (2020).
21. Forster, P. et al. in *Climate Change 2021: The Physical Science Basis* (eds Masson-Delmotte, V. et al.) 923–1054 (Cambridge Univ. Press, 2021).
22. Seidel, D. J., Gillett, N. P., Lanzante, J. R., Shine, K. P. & Thorne, P. W. Stratospheric temperature trends: our evolving understanding. *WIREs Clim. Change* **2**, 592–616 (2011).
23. Goessling, H. & Bathiany, S. Why CO_2 cools the middle atmosphere–a consolidating model perspective. *Earth Syst. Dyn.* **7**, 697–715 (2016).
24. Rodgers, C. D. & Walshaw, C. D. The computation of infra-red cooling rate in planetary atmospheres. *Q. J. R. Meteorolog. Soc.* **92**, 67–92 (1966).
25. Jeevanjee, N. & Fueglistaler, S. On the cooling-to-space approximation. *J. Atmos. Sci.* **77**, 465–478 (2020).
26. Jeevanjee, N. & Fueglistaler, S. Simple spectral models for atmospheric radiative cooling. *J. Atmos. Sci.* **77**, 479–497 (2020).
27. Cohen, S. & Pincus, R. A spectroscopic theory for how mean rainfall changes with surface temperature. *Sci. Adv.* **11** (2025).
28. Wordsworth, R., Seeley, J. T. & Shine, K. P. Fermi resonance and the quantum mechanical basis of global warming. *Planet. Sci. J.* **5**, 67 (2024).
29. Koll, D. D. B., Jeevanjee, N. & Lutsko, N. J. An analytic model for the clear-sky longwave feedback. *J. Atmos. Sci.* **80**, 1923–1951 (2023).
30. Wilson, D. J. & Gea-Banacloche, J. Simple model to estimate the contribution of atmospheric CO_2 to the earth's greenhouse effect. *Am. J. Phys.* **80**, 306–315 (2012).
31. Jeevanjee, N., Seeley, J. T., Paynter, D. & Fueglistaler, S. An analytical model for spatially varying clear-sky CO_2 forcing. *J. Clim.* **34**, 1–55 (2021).
32. Fildier, B., Muller, C., Pincus, R. & Fueglistaler, S. How moisture shapes low-level radiative cooling in subsidence regimes. *AGU Adv.* **4**, e2023AV000880 (2023).
33. Ramanathan, V. & Dickinson, R. E. The role of stratospheric ozone in the zonal and seasonal radiative energy balance of the earth-troposphere system. *J. Atmos. Sci.* **36**, 1084–1104 (1979).
34. Pinnock, S., Hurley, M. D., Shine, K. P., Wallington, T. J. & Smyth, T. J. Radiative forcing of climate by hydrochlorofluorocarbons and hydrofluorocarbons. *J. Geophys. Res.: Atmos.* **100**, 23227–23238 (1995).
35. Shine, K. P. & Myhre, G. The spectral nature of stratospheric temperature adjustment and its application to halocarbon radiative forcing. *J. Adv. Model. Earth Syst.* **12**, e2019MS001951 (2020).
36. Chapman, S. A theory of upper atmospheric ozone. *Mem. R. Meteorolog. Soc.* **3**, 103–125 (1930).
37. Chiodo, G. & Polvani, L. M. The response of the ozone layer to quadrupled CO_2 concentrations: implications for climate. *J. Clim.* **32**, 7629–7642 (2019).
38. Butchart, N. The Brewer-Dobson circulation. *Rev. Geophys.* **52**, 157–184 (2014).
39. Sherwood, S. C. et al. Adjustments in the forcing-feedback framework for understanding climate change. *Bull. Am. Meteorolog. Soc.* **96**, 217–228 (2015).
40. Forster, P. et al. Recommendations for diagnosing effective radiative forcing from climate models for CMIP6: recommended effective radiative forcing. *J. Geophys. Res.: Atmos.* **121** (2016).
41. Ramaswamy, V. et al. Radiative forcing of climate: the historical evolution of the radiative forcing concept, the forcing agents and their quantification, and applications. *Meteorolog. Monogr.* **59** (2019).
42. He, H., Kramer, R. J., Soden, B. J. & Jeevanjee, N. State dependence of CO_2 forcing and its implications for climate sensitivity. *Science* **382**, 1051–1056 (2023).
43. Smith, C. J. et al. Understanding rapid adjustments to diverse forcing agents. *Geophys. Res. Lett.* **45**, 12,023–12,031 (2018).
44. Maycock, A. C. et al. Revisiting the mystery of recent stratospheric temperature trends. *Geophys. Res. Lett.* **45**, 9919–9933 (2018).
45. Zou, C.-Z. & Qian, H. Stratospheric temperature climate data record from merged ssu and AMSU-A observations. *J. Atmos. Oceanic Technol.* **33**, 1967–1984 (2016).

Methods

Throughout most of the stratosphere, radiative exchange with the surface and the surrounding atmosphere largely cancel such that heating by CO_2 (H_{CO_2}) is dominated by longwave emission to space (Extended Data Fig. 2). Under the cooling-to-space (CTS) approximation, the spectrally resolved longwave heating rate H_ν at a given wavenumber ν and pressure level p is given by:

$$H_\nu = -\frac{g}{c_p}\pi B(T,\nu)\frac{\beta_\nu}{p}\tau_\nu e^{-\tau} \tag{10}$$

where g is the acceleration due to gravity, c_p is the specific heat of air, $B(T,\nu)$ is the Planck function, T is the temperature at p and $\beta_\nu = \frac{d\ln\tau_\nu}{d\ln p}$ is a measure of how quickly optical depth (τ_ν) changes with pressure[26]. For a well-mixed and pressure-broadened gas such as CO_2, which has $\beta_\nu = 2$, optical depth is well approximated by:

$$\tau_\nu = \frac{Dqk_{ref}(\nu)p^2}{2gp_{ref}} \tag{11}$$

where q is the concentration of CO_2, D is a diffusivity factor that approximates the angularly integrated flux and $k_{ref}(\nu)$ is the mass absorption coefficient of CO_2 at some reference pressure p_{ref} (ref. 31). Integration in ν across the CO_2 band yields H_{CO_2}, the total contribution of CO_2 to the longwave heating rate. Because variations in the Planck function across the CO_2 band are small, we can remove $B(T,\nu)$ from the spectral integral[26] to obtain equation (1):

$$H_{CO_2} = -\frac{2g}{pc_p}\pi B(T,\nu_0)l(p,q) \tag{12}$$

where ν_0 is the Planck function evaluated at the wavenumber at the centre of the CO_2 band (667.5 cm^{-1}) and

$$l(p,q) = \int_{CO_2} \tau_\nu e^{-\tau_\nu} d\nu \tag{13}$$

is CO_2's Goldilocks width (equivalent to equation (2)).

The validity of the cooling-to-space (CTS) approximation is closely tied to the rate at which Planck emission changes with optical depth[25]. If $\gamma = \frac{d\ln B}{d\ln\tau}$ is small (on the order of ≈ 0.1), the CTS approximation is rather strong; as γ increases, the CTS approximation breaks down. Because CO_2 is well mixed and because the lapse rate Γ in the stratosphere is roughly 1.5 km K^{-1}, stratospheric emission from the CO_2 band (where $\alpha = \frac{d\ln B}{d\ln T} \approx 4$) changes slowly with optical depth[25]:

$$\gamma_{CO_2} = \frac{d\ln B}{d\ln\tau} = \frac{d\ln B}{d\ln T}\frac{d\ln T}{d\ln p}\frac{d\ln p}{d\ln\tau} = \alpha\frac{R_d\Gamma}{g}\frac{1}{\beta} \approx 4\frac{287\,J\,kg^{-1}\,K^{-1}(1.5\,K\,km^{-1})}{9.8\,ms^{-2}}\frac{1}{2} \approx 0.09 \tag{14}$$

Here R_d is specific gas constant for dry air. Equation (14) suggests the CTS approximation is a suitable first-order approximation for the local longwave heating rate due to CO_2 in the stratosphere, a finding in line with previous studies[24,25,46] and validated by direct comparison to line-by-line computations in Konrad (Extended Data Fig. 2a).

Due to the linearity implicit in the construction of equation (14), the validity of the CTS approximation breaks down near temperature inversions such as the stratopause and tropopause (Extended Data Fig. 2a) where contributions from the inter-atmospheric exchange are large[25]. However, because changes in CO_2 concentration yield similar changes in temperature above and below these temperature inversions, radiative heating from the surrounding atmosphere is largely invariant to changes in CO_2 concentration q, making equation (3) a good approximation for $\frac{dH_{CO_2}}{d\ln q}$, even at the stratopause and tropopause (Extended Data Fig. 2b).

Unlike CO_2, ozone is not well mixed. In the upper stratosphere, where ozone concentration increases with pressure, β_{O_3} is substantially greater than unity, meaning $\gamma_{O_3} << 1$. Here the local longwave heating rate due to ozone is well approximated by CTS (Extended Data Fig. 5). In the lower stratosphere, where ozone concentration decreases with pressure, β_{O_3} is substantially smaller than unity, meaning $\gamma_{O_3} >> 1$, and the CTS approximation breaks down (Extended Data Fig. 5).

When the CO_2 concentration rises, CO_2's Goldilocks width $l(p,q)$ and, by extension, its longwave cooling rate H_{CO_2} increase in a height-dependent manner. Under the CTS approximation, this is given by:

$$\frac{dH_{CO_2}}{d\ln q} = -\frac{2g}{pc_p}\pi\left(B(T,\nu_0)\frac{dl(p,q)}{d\ln q} + \frac{dB(T,\nu_0)}{d\ln T}\frac{d\ln T}{d\ln q}l(p,q)\right) \tag{15}$$

which simplifies to equation (3):

$$\frac{d\ln H_{CO_2}}{d\ln q} = \frac{d\ln l(p,q)}{d\ln q} + \frac{d\ln B(T,\nu_0)}{d\ln T}\frac{d\ln T}{d\ln q} \tag{16}$$

Because global-mean annual stratospheric temperature is primarily controlled by radiative equilibrium, any transient change in longwave heating by CO_2 caused by an increase in CO_2 concentration must eventually be balanced by an equal and opposite change in longwave and shortwave heating by other radiatively active gases H_o, namely ozone and water vapour. This yields equation (4):

$$\frac{dH_{CO_2}}{dlnq} = -\frac{dH_o}{dlnq} \tag{17}$$

Because changes in q do not directly affect H_o but rather only influence H_o through their indirect impact on temperature, we can write $\frac{dH_o}{d\ln q}$ as:

$$\frac{dH_o}{d\ln q} = \frac{dH_o}{d\ln T}\frac{d\ln T}{d\ln q} \tag{18}$$

When combined, equations (16), (17) and (18) yield:

$$\frac{dH_o}{d\ln T}\frac{d\ln T}{d\ln q} = -H_{CO_2}\left(\frac{d\ln l(p,q)}{d\ln q} + \frac{d\ln B(T,\nu_0)}{d\ln T}\frac{d\ln T}{d\ln q}\right) \tag{19}$$

Solving for $\frac{d\ln T}{d\ln q}$, we obtain:

$$\frac{d\ln T}{d\ln q} = -\left(\frac{\eta}{\alpha}\right)\frac{d\ln l(p,q)}{d\ln q} \tag{20}$$

where $\alpha = \frac{d\ln B(T,\nu_0)}{d\ln T}$ (ref. 25) and $\eta = \frac{dH_{CO_2}}{dT}/\frac{d(H_{CO_2}+H_o)}{dT}$. When discretized over some change in CO_2 concentration, equation (20) yields equation (5).

Armed with a governing equation for stratospheric temperature, we need only approximations for Goldilocks width ($l(p,q)$) and the change in longwave heating by ozone and water vapour with temperature ($\frac{dH_o}{dT}$) to complete our simple model for CO_2-induced stratospheric cooling.

To approximate $l(p,q)$, we use the spectroscopy of CO_2 to assess how many wavenumbers have $\tau_\nu = 1$ at a given pressure level p. By binning the logarithm of the mass absorption coefficient of CO_2 $k_{ref}(\nu)$ (Fig. 2c, grey), we can count how many wavenumbers in the CO_2 band have a given mass absorption coefficient (or one quite close to it) at our reference pressure of 100 hPa (ref. 47). This effectively replaces l's integrand $\tau_\nu e^{-\tau_\nu}$ with a Dirac delta function centred at $\tau_\nu = 1$ (ref. 26):

$$\begin{aligned} l(p,q) &= \int \tau_\nu e^{-\tau}\, d\nu \approx \int \delta(1-\tau_\nu)d\nu = \frac{1}{\left|\frac{d\ln\tau_\nu}{d\nu}\right|_{\tau_\nu=1}} \\ &= \frac{1}{\left|\frac{d\ln k_{ref}}{d\nu}\right|_{\tau_\nu=1}} = l(k_{ref})|_{\tau_\nu=1} \end{aligned} \tag{21}$$

where the quantity $l(k_{ref}) = \left|\frac{d\nu}{d\ln k_{ref}}\right|$ approximates the Goldilocks width of CO_2 at the pressure level associated with k_{ref}, that is, at the pressure

level where k_{ref} yields $\tau_\nu = 1$ (ref. 47). Assuming k_{ref} is monotonic in ν, an assumption that is observably false for the CO_2 band (Fig. 2a, grey) but that can be made without loss of generality, $l(k_{ref}) = |\frac{d\nu}{d\ln k_{ref}}|$ will be given by the PDF of $\ln k_{ref}$ (Fig. 2c, grey). We parameterize $l(k_{ref})$ using the following form:

$$l(k_{ref}) = 2l_0\left(1 - e^{-\left(\frac{k_0}{k_{ref}}\right)^a}\right) \tag{22}$$

Here l_0, k_0 and a are shape parameters (Fig. 2a–c, dashed black); l_0 and k_0 are taken from previous parameterizations of CO_2's spectroscopy[27,29,31] and a is derived by fitting equation (22) to binned values in Fig. 2c. The Goldilocks fraction $l(p, q)$ is therefore the mass absorption coefficient that (using equation (11)) yields $\tau_\nu = 1$ at pressure p:

$$l(p,q) = 2l_0\left(1 - e^{-\left(\frac{Dqk_0p^2}{2gp_{ref}}\right)^a}\right) \tag{23}$$

Similarly, to capture the impact of water vapour and ozone on CO_2-induced stratospheric cooling, we use the following empirical parameterization:

$$\frac{dH_o}{dT} = C_{strat}\cos\left(\frac{\pi}{2}\left(\frac{p - p_{strat}}{p_{tropo} - p_{strat}}\right)\right)^2 \tag{24}$$

Here p_{strat} is the pressure at the stratopause, p_{tropo} is the pressure at the tropopause and C_{strat} is a constant obtained by fitting equation (24) to changes in temperature and radiative heating derived from simulations in Konrad (Extended Data Fig. 5). Equation (24) assumes that the combined radiative heating rate of ozone and water vapour scales linearly with local temperature at each pressure level ($\frac{dH_o}{dT} = f(p)$), neglecting the nonlinear growth of Planck emission with temperature and the non-local effect of changes in inter-atmospheric radiative exchange.

Together, equations (5), (23) and (24) form our simple model for CO_2-induced stratospheric cooling. For reference, Extended Data Table 1 lists all of the spectroscopic parameters used in our idealized models.

One important implication of stratospheric cooling is its impact on CO_2's radiative forcing[3,39–41]. To estimate the effective (or, more precisely, the stratosphere-adjusted) radiative forcing, we begin by considering the change in outgoing longwave radiation OLR due to some change in q:

$$\frac{dOLR}{d\ln q} = -\frac{d}{d\ln q}\int_0^\infty \pi B(T_{em}(\nu),\nu)d\nu \tag{25}$$

Here $T_{em}(\nu)$ is the emission temperature at each wavenumber and is well approximated by the temperature at the pressure level where optical depth is unity and by the surface temperature where the column optical depth is less than unity[25]. Assuming surface and tropospheric temperatures remain fixed, we can expand equation (25) to delineate contributions to changes in OLR from each of the radiatively active gases in the stratosphere:

$$\begin{aligned}\frac{dOLR}{d\ln q} = -\frac{d}{d\ln q}\Bigg(&\int_{CO_2}\pi B(T_{em}(\nu),\nu)d\nu \\ &+\int_{O_3}\pi B(T_{em}(\nu),\nu)d\nu + \int_{H_2O}\pi B(T_{em}(\nu),\nu)d\nu\Bigg)\end{aligned} \tag{26}$$

As CO_2 concentration increases, the CO_2 band widens; for each factor of e increase in CO_2 concentration, each side of the CO_2 band widens by l_0, masking the surface and tropospheric emission at the edges of the CO_2 band[31]. By definition of l and β, within each band $d\nu = l d\ln k_{ref} = -\beta l d\ln p$, allowing us to integrate in (emission) pressure rather than wavenumber. Because variations in the Planck function across the CO_2, ozone and water vapour bands are small, we let $B(T_{em}(\nu), \nu) = B(T_{em}(\nu), \nu_0)$ in each band, where ν_0 is the band's central wavenumber[25]:

$$\frac{dOLR}{d\ln q} = -2\pi l_0 B(T(\bar{p}),\nu_{0,CO_2}) + \int_0^{\bar{p}}\frac{d}{d\ln q}\left(\sum_i^{CO_2,O_3,H_2O}\pi B(T(p),\nu_{0,i})\beta_i l_i\right)d\ln p \tag{27}$$

Here the average emission temperature at the edges of the CO_2 band $\bar{T} = T(\bar{p})$[31] is calculated in the same manner as T_{em} in equation (10) of ref. 27. Whereas emission by CO_2 is impacted by both changes in l_{CO_2} and changes in stratospheric temperature, only the latter affects emission by ozone and water vapour. Combining equation (27) with equations (4) and (20) yields:

$$\begin{aligned}\frac{dOLR}{d\ln q} &= -2\pi l_0 B(T(\bar{p}),\nu_{0,CO_2}) \\ &+\int_0^{\bar{p}}\beta_{CO_2}(1-\eta_{CTS})\pi B(T(p),\nu_{0,CO_2})\frac{dl_{CO_2}}{d\ln q}d\ln p\end{aligned} \tag{28}$$

where $\eta_{CTS} = \frac{dH_{CTS}}{dT}/\frac{dH_{total}}{dT}$ is a 'cooling-to-space spectral efficiency' that measures what fraction of the total change in longwave cooling comes from changes in cooling to space. Because CTS is a suitable approximation for CO_2 throughout the depth of the stratosphere but a poor approximation for ozone in the lower stratosphere (where almost all stratospheric emission to space comes from), assuming $\eta_{CTS} \approx \eta = \frac{dH_{CO_2}}{dT}/\frac{dH_{total}}{dT}$ yields a first-order estimate of ERF (even though η_{CTS} is substantially greater than η in the upper stratosphere; Extended Data Fig. 6). Because ERF = −ΔOLR, discretizing equation (28) over some change in CO_2 concentration (and letting $\eta_{CTS} = \eta$) yields equation (7).

When the reduced emission to space from ozone and water vapour due to stratospheric cooling is accounted for, the stratospheric adjustment is roughly 20% greater (Extended Data Figs. 8 and 9). Interestingly, if CTS were a suitable approximation for all radiatively active gases in the stratosphere ($\eta_{CTS} \approx 1$), stratospheric emission to space would be invariant to changes in CO_2 concentration and stratospheric temperature insofar as shortwave heating, which this emission must balance, remains constant. In this case, ERF would simply be given by the masked surface emission (that is, ERF_{max}). Note that in our emission level approximations of both radiative forcing and longwave radiative cooling, we assume emission is dominated by the $\tau = 1$ pressure level. In reality, the pressure level representative of net cooling to space and the pressure level where radiative cooling is maximized are not necessarily equivalent to the $\tau = 1$ pressure level[25,31]. Because these corrections do not substantially improve our simulation of stratospheric cooling and radiative forcing, we use the $\tau = 1$ pressure level for simplicity.

Data availability

All data used in constructing this study's figures are available via Zenodo at https://doi.org/10.5281/zenodo.16929030 (ref. 48).

References

46. Schwarzkopf, M. D. & Fels, S. B. The simplified exchange method revisited: an accurate, rapid method for computation of infrared cooling rates and fluxes. *J. Geophys. Res.: Atmos.* **96**, 9075–9096 (1991).
47. McKim, B. A., Jeevanjee, N., Vallis, G. K. & Lewis, N. T. Water vapor spectroscopy and thermodynamics constrain earth's tropopause temperature. *AGU Adv.* **6**, e2024AV001206 (2025).
48. Cohen, S. Raw data and plotting code for 'why increases in CO_2 cool the stratosphere and how this amplifies radiative forcing'. *Zenodo* https://doi.org/10.5281/zenodo.16929030 (2026).

Acknowledgements

We thank I. Mitevski, A. Williams and M. Powell for helpful feedback during various stages of this work. We are grateful for support from the

National Science Foundation under award AGS-1916908 (S.C. and R.P.), AGS 25-36164 (R.P.), and AGS-2335762 (S.C., L.M.P.). We also thank N. Jeevanjee and H. He for providing constructive feedback on this paper.

Author contributions

S.C., R.P. and L.M.P. designed research; S.C. performed research; S.C. analysed data and S.C., R.P. and L.M.P. wrote the paper.

Competing interests

The authors declare no competing interests.

Additional information

Extended data is available for this paper at https://doi.org/10.1038/s41561-026-01965-8.

Supplementary information The online version contains supplementary material available at https://doi.org/10.1038/s41561-026-01965-8.

Correspondence and requests for materials should be addressed to Sean Cohen.

Peer review information *Nature Geoscience* thanks Michael Byrne, Haozhe He and Nadir Jeevanjee for their contribution to the peer review of this work. Peer reviewer reports are available. Primary Handling Editor: Aliénor Lavergne, in collaboration with the *Nature Geoscience* team.

https://doi.org/10.1038/s41561-026-01965-8

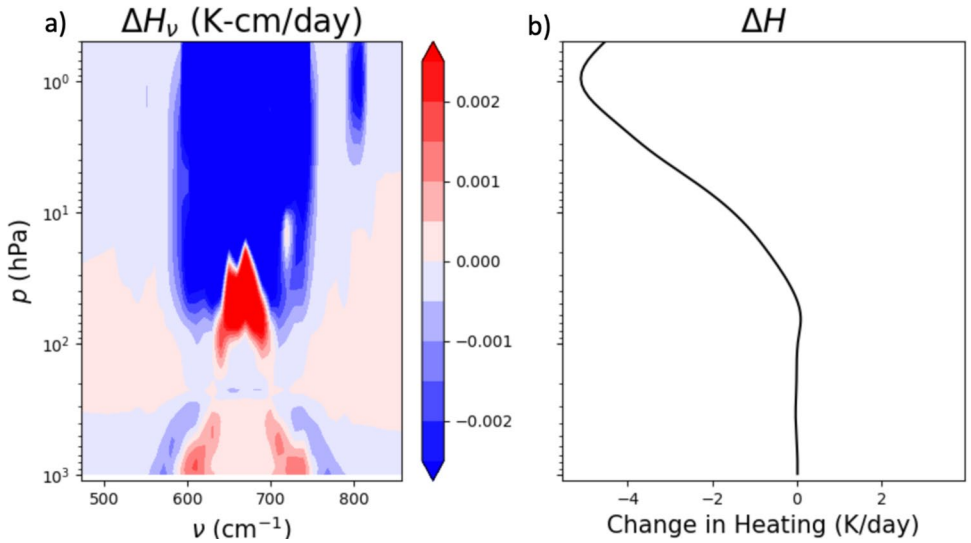

Extended Data Fig. 1 | Changes in CO_2 do not affect tropospheric heating by CO_2. (**a**) Spectrally resolved and (**b**) spectrally integrated change in heating across the CO_2 band when CO_2 concentration is quadruped from pre-industrial. CO_2 is the only absorber and temperature is held fixed to the profile which yields radiative convective equilibrium under pre-industrial CO_2 concentration (black line in Fig. 1a).

https://doi.org/10.1038/s41561-026-01965-8

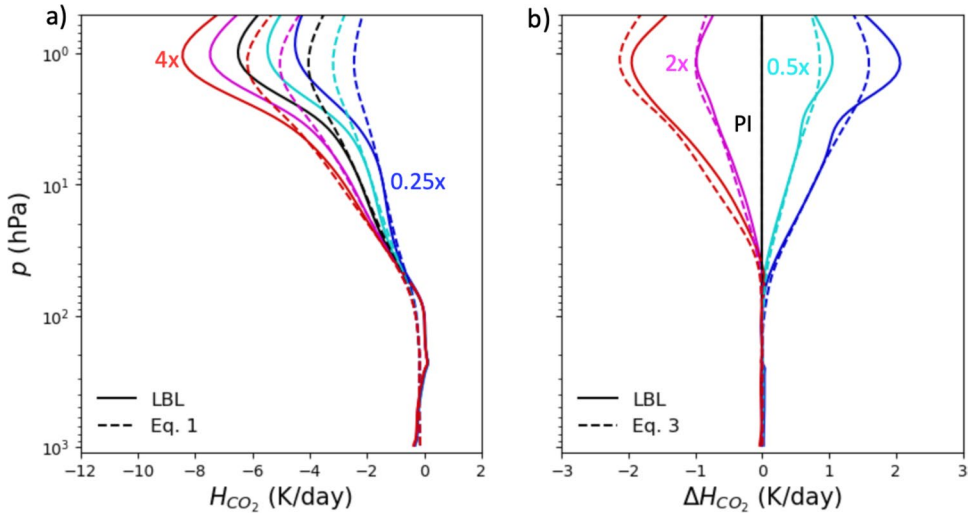

Extended Data Fig. 2 | Stratospheric longwave emission by CO_2 is dominated by cooling-to-space. (**a**) Heating by CO_2 under pre-industrial CO_2 concentration (black) and under subsequent doublings (warmer colours) and halvings (cooler colours) of CO_2 concentration from pre-industrial (PI) levels. Line-by-line simulations in Konrad (solid) are compared to Eq. 1 (dashed), an analytical expression derived using the CTS approximation. The CTS approximation is a suitable first-order approximation for H_{CO_2} in most of the stratosphere but breaks down near temperature inversions like the stratopause and tropopause. (**b**) However, because changes in CO_2 concentration yield similar changes in temperature above and below these temperature inversions, the CTS approximation (Eq. 3) generally captures the change in heating by CO_2 with CO_2 concentration (same colours and line types) near the stratopause and tropopause.

https://doi.org/10.1038/s41561-026-01965-8

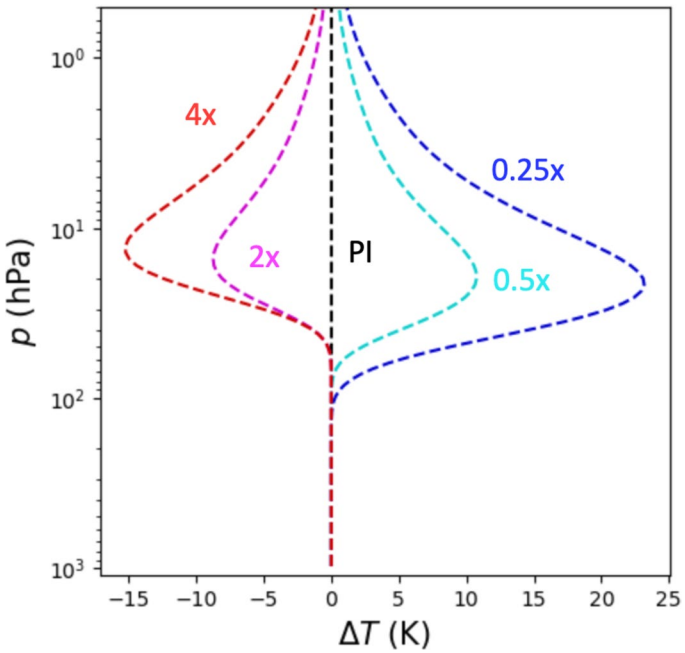

Extended Data Fig. 3 | Linear parameterizations of CO_2's spectroscopy do not capture the vertical structure of stratospheric cooling. Stratospheric temperature change from pre-industrial conditions (black) under subsequent doublings (warmer colours) and halvings (cooler colours) of CO_2 concentration implied by the linear parameterization of CO_2's spectroscopy. Due to the sharp transition in Goldilocks width at the parameterization's maximum value of k_{ref}, stratospheric cooling is amplified near this transition and near zero elsewhere. This transition is infinitely sharp when l is approximated using a Dirac delta function (as in Fig. 2c), but is also apparent when Goldilocks width is computed explicitly (as above).

https://doi.org/10.1038/s41561-026-01965-8

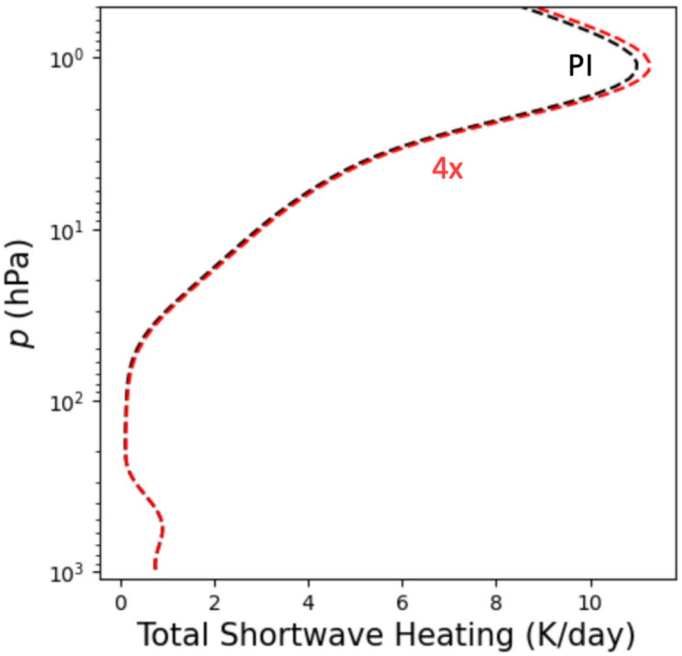

Extended Data Fig. 4 | Shortwave heating is largely invariant to changes in CO_2 concentration. Spectrally integrated shortwave heating rate under pre-industrial CO_2 concentration (black) and after a quadrupling of CO_2 from PI (red).

https://doi.org/10.1038/s41561-026-01965-8

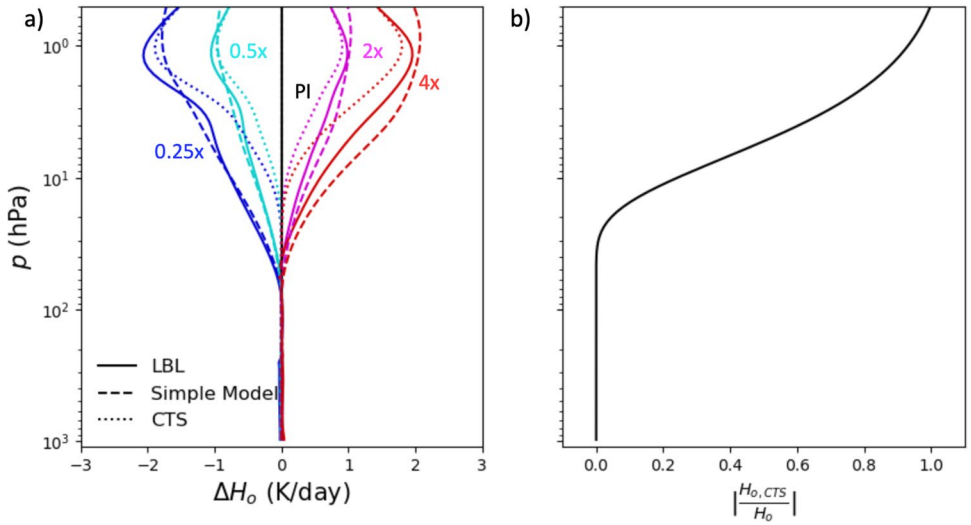

Extended Data Fig. 5 | The combined radiative heating rate of ozone and water vapour scales roughly linearly with local temperature and is poorly approximated by cooling-to-space in the lower stratosphere. (**a**) Change in water vapour and ozone's spectrally integrated heating rate from pre-industrial CO_2 concentration (black) under subsequent doublings (warmer colours) and halvings (cooler colours) of CO_2 concentration. We compare our idealized model (dashed) to RCE simulations in Konrad (solid). While more accurate in the upper stratosphere, the cooling-to-space approximation (dotted) breaks down in the lower stratosphere. (**b**) Averaged across all simulations, emission to space by ozone and water vapour captures less than 20% of the total longwave cooling below 10hPa.

https://doi.org/10.1038/s41561-026-01965-8

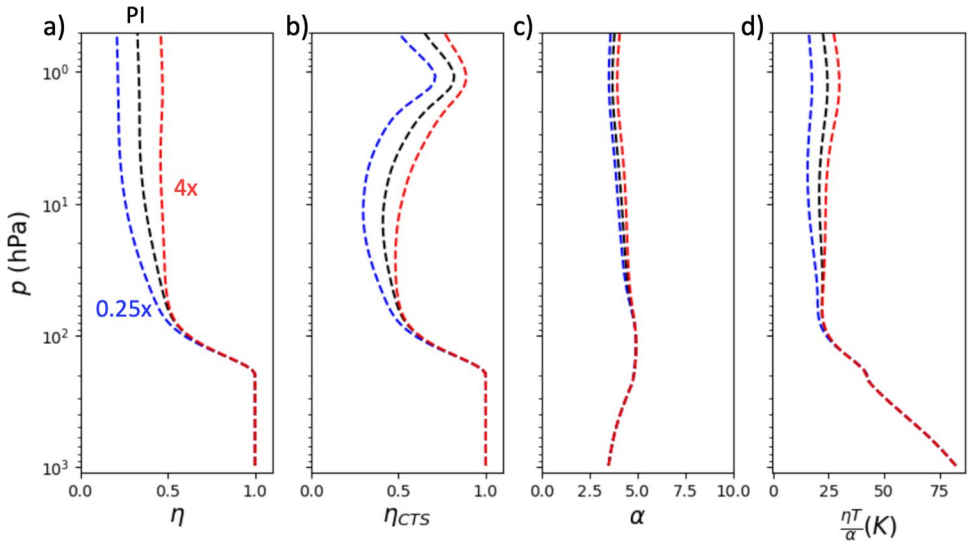

Extended Data Fig. 6 | Spectral efficiency and source scaling are nearly constant throughout the depth of the stratosphere, but cooling-to-space spectral efficiency is not. (**a**) Spectral efficiency η (**c**) source scaling α, and (**d**) the combined effect of these quantities on stratospheric cooling $\frac{\eta T}{\alpha}$ across the depth of the stratosphere for pre-industrial CO_2 concentration (black) and for a quadrupling (red) and a quartering (blue) of CO_2 from PI. (**b**) Cooling-to-space spectral efficiency η_{CTS} is substantially greater than η in the upper stratosphere and approximately equal to η in the lower stratosphere. Since most stratospheric emission to space originates from the lower stratosphere, assuming $\eta_{CTS} \approx \eta$ yields a first-order estimate of effective radiative forcing.

https://doi.org/10.1038/s41561-026-01965-8

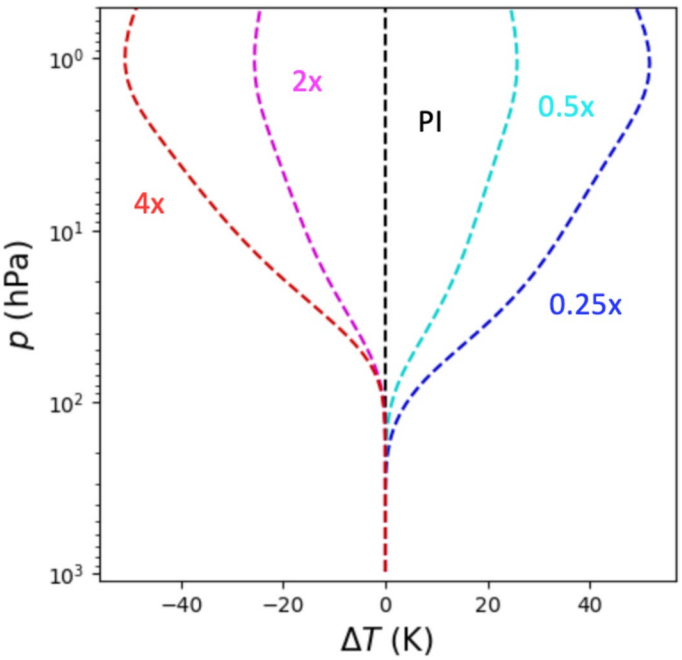

Extended Data Fig. 7 | Stratospheric cooling is amplified when longwave emission by ozone and water vapour is held constant. Stratospheric temperature change from pre-industrial conditions (black) under subsequent doublings (warmer colours) and halvings (cooler colours) of CO_2 concentration when longwave emission by ozone and water vapour is held constant.

https://doi.org/10.1038/s41561-026-01965-8

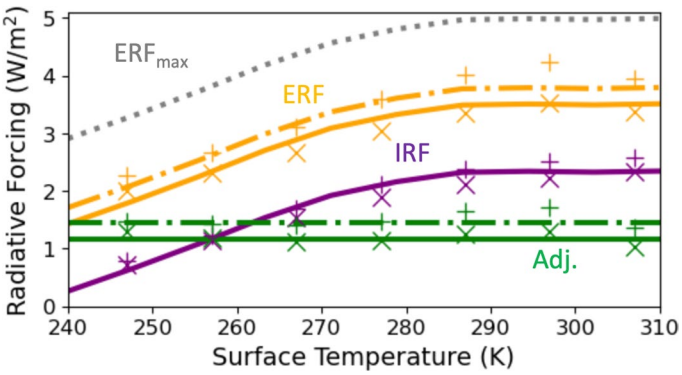

Extended Data Fig. 8 | Changes in emission to space by ozone and water vapour increase the magnitude of the stratospheric adjustment. As in Fig. 5, but with radiative forcing calculations across the entire spectrum included (Eq. 28 = dash dot lines, line-by-line computations in Konrad = pluses). To account for the reduction in emission by ozone and water vapour as the stratosphere cools, we use η_{CTS} which is roughly equal to η in the lower stratosphere, but substantially larger than η in the upper stratosphere (Extended Data Fig. 6).

https://doi.org/10.1038/s41561-026-01965-8

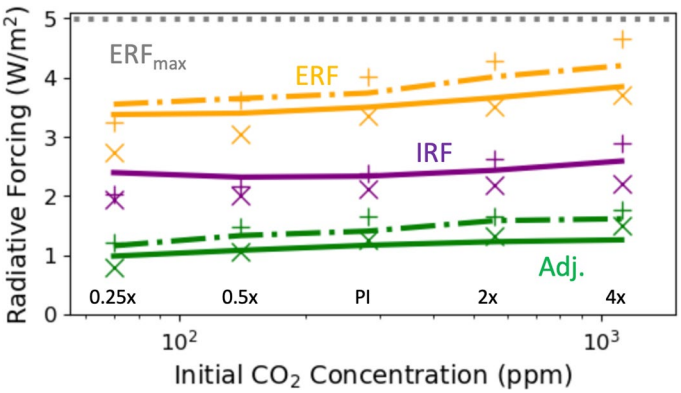

Extended Data Fig. 9 | The magnitude of the stratospheric adjustment changes relatively little with CO_2 concentration. Radiative forcing across the CO_2 band due to doubling of CO_2 under 0.25x, 0.5x, 1x, 2x, and 4x pre-industrial CO_2 concentration. In all runs, surface temperature is held fixed to 287K. Line-by-line computations in Konrad (crosses) are compared to Eq. 7 (solid lines). Effective radiative forcing (orange) falls about halfway between the instantaneous radiative forcing (purple) and a theoretical maximum radiative forcing (grey, Eq. 8) where ozone and water vapour do not mute stratospheric cooling. The magnitude of the stratospheric adjustment is shown in green. As in Extended Data Fig. 8, accounting for the reduction in emission elsewhere in the spectrum (Eq. 28 = dash dot lines, line-by-line computations in Konrad = pluses) increases the stratospheric adjustment by about 20%. As CO_2 concentration increases, CO_2's 1000cm^{-1} bands, which our model neglects, become more emissive (difference between purple crosses and pluses). Note that, using RRTMG in Konrad, ref. 18 found a weak negative relationship between CO_2 concentration and the stratospheric adjustment; given that ref. 18 also found the magnitude of the stratospheric adjustment to be somewhat sensitive to the computational method used, this discrepancy may be due to differences in RRTMG and line-by-line computations in ARTS.

https://doi.org/10.1038/s41561-026-01965-8

Extended Data Table 1 | List of parameters used in our simple model

Parameter	Description	Assumed Value
D	Diffusivity factor	5/3
p_{tropo}	Tropopause pressure level	200 hPa
p_{tropo}	Stratopause pressure level	1 hPa
C_{strat}	Temperature sensitivity of H_o at the stratopause	-0.11 day^{-1}
k_0	Absorption cross-section at which $l(k_{\text{ref}})$ begins decaying	50 m^2/kg
l_0	Goldilocks width at edge of CO_2 band	10.2 cm^{-1}
a	Relative rate at which $l(k_{\text{ref}})$ decays with absorption cross-section	0.52
ν_0	Wavenumber of the peak of the CO_2 band	667.5 cm^{-1}

See methods section for details.